

- 3988

LA-UR-00-

97031

Approved for public release;  
distribution is unlimited

Title:

**Novel Signal Processing with Nonlinear  
Transmission Lines**

Author(s):

D. W. Reagor\* (MST-STC), A. T. Findikoglu (MST-STC),  
A. Bishop (T-11), N. Gronbech-Jensen (T-11),  
K. Ø. Rasmussen (T-11), D. Cai (T-11), Q. X. Jia (MST-STC),  
Y. Fan (MST-STC), C. Kwon (MST-STC), and  
L. A. Ostrovsky (University of Colorado, Boulder)

Submitted to:

DOE Office of Scientific and Technical Information (OSTI)

**Los Alamos**  
NATIONAL LABORATORY

Los Alamos National Laboratory, an affirmative action/equal opportunity employer, is operated by the University of California for the U.S. Department of Energy under contract W-7405-ENG-36. By acceptance of this article, the publisher recognizes that the U.S. Government retains a nonexclusive, royalty-free license to publish or reproduce the published form of this contribution, or to allow others to do so, for U.S. Government purposes. Los Alamos National Laboratory requests that the publisher identify this article as work performed under the auspices of the U.S. Department of Energy. Los Alamos National Laboratory strongly supports academic freedom and a researcher's right to publish; as an institution, however, the Laboratory does not endorse the viewpoint of a publication or guarantee its technical correctness.

## **DISCLAIMER**

**This report was prepared as an account of work sponsored by an agency of the United States Government. Neither the United States Government nor any agency thereof, nor any of their employees, make any warranty, express or implied, or assumes any legal liability or responsibility for the accuracy, completeness, or usefulness of any information, apparatus, product, or process disclosed, or represents that its use would not infringe privately owned rights. Reference herein to any specific commercial product, process, or service by trade name, trademark, manufacturer, or otherwise does not necessarily constitute or imply its endorsement, recommendation, or favoring by the United States Government or any agency thereof. The views and opinions of authors expressed herein do not necessarily state or reflect those of the United States Government or any agency thereof.**

## **DISCLAIMER**

**Portions of this document may be illegible in electronic image products. Images are produced from the best available original document.**

# Novel Signal Processing with Nonlinear Transmission Lines

D. W. Reagor\*, A. T. Findikoglu, A. Bishop, N. Gronbech-Jensen,  
K. Ø. Rasmussen, D. Cai, Q. X. Jia, Y. Fan, C. Kwon, and  
L. A. Ostrovsky (University of Colorado, Boulder)

RECEIVED

DEC 13 2000

OSTI

## Abstract

Nonlinear dielectrics offer uniquely strong and tunable nonlinearities that make them attractive for current devices (for example, frequency-agile microwave filters) and for future signal-processing technologies. The goal of this project is to understand pulse propagation on nonlinear coplanar waveguide prototype devices. We have performed time-domain and frequency-domain experimental studies of simple waveguide structures and pursued a theoretical understanding of the propagation of signals on these nonlinear waveguides.

To realistically assess the potential applications, we used a time-domain measurement and analysis technique developed during this project to perform a broadband electrodynamic characterization in terms of nonlinear, dispersive, and dissipative effects. We completed a comprehensive study of coplanar waveguides made from high-temperature superconducting thin-film  $\text{YBa}_2\text{Cu}_3\text{O}_{7-\delta}$  electrodes on nonlinear dielectric single-crystal  $\text{SrTiO}_3$  substrates. By using parameters determined from small-signal (linear) transmission characteristics of the waveguides, we develop a model equation that successfully predicts and describes large-signal (nonlinear) behavior.

## Background and Research Objectives

The established methods in communications typically use a narrow spectral range. For example, VHF TV stations operate in bandwidths of 6 MHz on at least a 60 MHz carrier. Frequency modulated (FM) radio uses less than 100 kHz bandwidth on carriers of order 100 MHz. Standard cellular phones use a wide band of carriers but each active transmitter is only allocated a narrow bandwidth around the carrier.

These standard methods introduce many well-established problems. First, if interference exists due to proximity of a high power transmitter or a system out of compliance, then a narrowband system will be jammed with a relatively small amount of power. Scattering sources such as large structures create a standing wave pattern in their vicinity. At the null points of the standing wave no signal is received, an effect called multipath fading. In addition, placing all the information in a narrow range of frequencies allows interception by unauthorized receivers. Also, in radar, one of the main drivers of high frequency applications, the narrowband systems return little information on the spatial structure of the scattering source.

---

\*Principal Investigator, e-mail: reagor@lanl.gov

To overcome the shortcomings of narrowband techniques, systems are evolving towards wide bandwidths and greater time domain character. One such technique is spread-spectrum, where information is sent at various frequencies and the receiver only tracks the frequency of transmission at any given time. In time-domain-multiple-access the transmitters send a short high bandwidth packet then wait for other transmitters to send packets. From the point of view of information theory or wave propagation, these wide bandwidth techniques are far superior and attracting wide interest. However, providing sufficiently high performance electronics for future generations of such wide bandwidth systems is an unsolved problem.

### **Importance to LANL's Science and Technology Base and National R&D Needs**

The research on HTS materials at LANL is part of the nuclear and advanced materials competency. In addition, the extreme sensitivity of the HTS electronics allows new types of high performance measurements, a contribution to the complex experiments and measurements competency.

This project has developed the HTS technology necessary for other potential programs and products. The major areas of application are communications and radar systems. A DOD agency has expressed interest in the work discussed here and may be a further source of funding. Beyond these communications problems, HTS electronics has been recognized by numerous agencies as a technology of the future.

### **Scientific Approach and Accomplishments**

The changing emphasis in High Temperature Superconductor (HTS) electronics research from single-layer thin films to multilayered thin film structures, has led to increasing interest in high-frequency applications of metal-oxide-based nonlinear dielectrics (NLDs), such as  $\text{SrTiO}_3$  (STO), in combination with HTS electrodes.<sup>1-3</sup> In essence, devices based on HTS/NLD structures promise to perform much better than their normal-metal/NLD predecessors due to: (i) reduced operational temperature leading to, in certain cases, lower dielectric loss, larger nonlinearity, and shorter relaxation times in the dielectric; (ii) lower conductor loss, and no intrinsic dispersion up to very high frequencies ( $\sim$ THz) in the superconducting electrodes; and (iii) "cleaner" electrode-dielectric interface leading to lower interface loss and negligible Schottky barriers.

These HTS/NLD structures are attractive not only for immediate implementation in practical devices such as frequency-agile microwave filters,<sup>4</sup> but also for the exploration of novel scientific and technological concepts such as study of stochastic effects and pulse-shaping.<sup>5</sup>

One of the most crucial features of this developing technology based on HTS/NLD structures is the ability to miniaturize substantially, i.e., to prepare compact devices. The importance of compact size for integration with other potential circuit components is clear. But, more importantly, since nonlinear effects in a dielectric are a function of the electric field applied to the dielectric, the smaller separation of electrodes allows for the realization of the same effects with smaller signal and control voltage levels. Whereas the dielectric loss is mostly determined by the loss tangent of the material irrespective of its size, the conductor loss, which is proportional to the surface resistance ( $R_s$ ) of the electrodes, increases strongly with decreasing conductor separation. Thus, the very low  $R_s$  of superconducting electrodes ( $\sim \mu\Omega$  below about 80 K at 1 GHz for  $\text{YBa}_2\text{Cu}_3\text{O}_{7-\delta}$  (YBCO)) permits designs of compact devices with practically low operational voltage levels ( $\sim 1$ -10 V).

Most potential applications would require thin films of both the NLD and the HTS material on an appropriate low-loss substrate. However, at present, even the highest quality NLD films show much smaller dielectric constant and nonlinearity, and higher dielectric losses than their single-crystal NLD counterparts.<sup>6</sup> Also, the functional dependence of dielectric properties on external electric field bias seems to be quite different in thin films (for example, whereas the dielectric loss decreases with bias in thin films, it increases in single crystals).<sup>7</sup> Currently, several approaches are being explored to make films with improved properties; such as chemical doping,<sup>8,9</sup> use of heteroepitaxial buffer layers,<sup>10</sup> and release of films from substrates by selective etching<sup>11</sup>. While the effort on improving the properties of NLD films continues, it is also important to explore, in parallel, device concepts using the single-crystals that possess intrinsic and more reproducible properties.

In the following, we will summarize our work on prototype nonlinear devices based on YBCO coplanar waveguide electrodes on single-crystal STO substrates. To facilitate extensive study of nonlinear and dispersive effects (which will be described later), we have adopted a time-domain measurement technique,<sup>12</sup> which allows for separation of dc-bias effects and high-frequency effects, and uses electrically-distributed transmission line concepts for analysis. The use of distributed coplanar waveguides has enabled us to investigate the high-frequency properties of STO single-crystals with high resolution because of the long interaction lengths.

Among several different lengths for the coplanar waveguide, 8-cm provided the best compromise between overall dissipation and cumulative nonlinear/dispersive effects.

## EXPERIMENT

A schematic of our coplanar waveguide device structure and its pertinent dimensions are shown in Fig. 1. The electrodes are 0.4- $\mu\text{m}$ -thick YBCO films, patterned in the form of 8-cm-long meandering coplanar waveguides. The YBCO films were pulsed-laser-deposited (from a stoichiometric target) on 1 cm x 1 cm x 1 mm (100) single-crystal STO substrates at a substrate temperature of 780 °C in 200 mTorr  $\text{O}_2$ . The pulsed laser used is a Xe-Cl excimer laser operating at 308-nm-wavelength with a repetition rate of 20 Hz and laser energy density of 2 J/cm<sup>2</sup> on the target. After deposition, the electrodes were defined by standard photolithography, and patterned by dilute phosphoric acid (500 ppm  $\text{H}_3\text{PO}_4$ ), followed by rf-sputtering of 0.5- $\mu\text{m}$ -thick Au contact pads on both ends of the centerline and groundplanes. As a last processing step, the devices were annealed at 400 °C for 12 h in flowing  $\text{O}_2$ .

Figure 2 shows the measurement set-up we used for broadband time-domain characterization of these nonlinear devices. The sample housing was designed specifically for these experiments: it uses a suspended-substrate geometry without side walls to reduce and attenuate unwanted housing modes; no external pressure is applied on the substrate to reduce complications due to possible piezoelectric effects (i.e., the substrate is un-clamped); short (~2 mm) coplanar waveguide segments with 50- $\Omega$  characteristic impedance are used as an intermediate adapter to guide broadband electromagnetic waves from cylindrical symmetry of the coaxial cable to coplanar waveguide symmetry of the device; and short (~1 mm) and low-inductance (~2 nH) Au wires are used to bond the electrodes of the device to the intermediate adapter.

The housing is clamped on a cold-head of a cryostat in a vacuum chamber. The input and output ports of the housing are connected with coaxial cables to the instruments outside the chamber via hermetically sealed connectors attached on ports of the chamber. The bias-Tees are essentially rf-chokes, which allow the dc bias to be separated from high-frequency signals. The high-frequency channel is a bandpass filter with 3-dB cut-off frequencies of 20 kHz and 12.5 GHz.

For our high-frequency device characterization, we have used two different measurement configurations; the standard step-pulse *time-domain-reflection/time-domain-transmission* (TDR/TDT) configuration, and the impulse-TDT configuration.

The impulse-*TDT* configuration (connection of which is shown in a dashed line in Fig. 2) uses a Gaussian-like pulse with about 0.4 ns full-width-at-half-maximum and with varying amplitudes (between 0.2 V and 40 V) as the excitation signal and monitors only the transmitted signal. The step-pulse *TDR/TDT* configuration has been best suited for the overall characterization of the devices in the small-signal limit, whereas impulse-*TDT* configuration has been essential for the study of nonlinear/dispersive effects in the large-signal limit.

### *ELECTRICAL CIRCUIT MODEL AND SMALL SIGNAL RESPONSE*

In the analysis of broadband characteristics of our devices, we will use an electrical circuit model based on lumped circuit element equivalents of coupling inductance  $L_c$  and input/output impedance  $Z_L$  for the external circuitry; and distributed element equivalents of series resistance  $R$ , series inductance  $L$ , shunt conductance  $G$ , and shunt capacitance  $C$  per unit length of the coplanar waveguide (see Fig. 3).

In their most general form, the inductance and impedance of the lumped elements are constants; and those of the distributed circuit elements depend on angular frequency  $\omega$ , temperature  $T$ , bias voltage  $v_{dc}$ , and signal voltage  $v_s$ . The characteristic impedance  $Z_o$  and propagation function  $\gamma$  of the coplanar waveguide are given by<sup>13</sup>

$$Z_o = \sqrt{(R + i\omega L)/(G + i\omega C)} \quad (1)$$

and

$$\gamma = \sqrt{(R + i\omega L)(G + i\omega C)} = \alpha + i\frac{\omega}{c}n \quad (2)$$

where  $c$  is the speed of light in vacuum,  $\alpha$  is the attenuation constant, and  $n$  is the effective refractive index. Assuming  $R$  and  $G$  are respectively much smaller than  $\omega L$  and  $\omega C$  (in other words, series and shunt losses are small), we obtain

$$n = c\sqrt{LC} \quad (3)$$



and

$$\alpha = \frac{R}{2\sqrt{L/C}} + \frac{G}{2\sqrt{C/L}}. \quad (4)$$

Physically,  $L$  and  $C$  are related to the magnetic and the electric field energy stored in the waveguide, respectively.  $C$  is solely determined by the shunt geometric capacitance of the waveguide, whereas  $L$  has contributions both from the series geometric inductance of the waveguide and the surface inductance of the electrodes.  $R$  signifies dissipative losses in the series channel and is dominated by the surface resistance of the YBCO electrodes.  $G$  combines both the dissipative losses in the dielectric medium and the radiative losses through the dielectric. As will be described later, various approximations will be necessary to calculate these parameters under specific conditions.

To quantify linear dispersive and dissipative effects, one can examine spectral components of the step-pulse *TDR/TDT* response. This has been done in detail<sup>14</sup> on these devices. Here we will only present the results with an equivalent method, impulse *TDT* analysis. We prefer impulse *TDT* in anticipation of the fact that, for the study of nonlinear effects described in the following, one needs large amplitude signals, which are not as readily available in the form of short-risetime step-pulses. Furthermore, Gaussian-like impulses are similar to microwave soliton solutions of many nonlinear/dispersive systems, and thus can be used as incident pulses to investigate soliton-supporting characteristics of our waveguides.<sup>15</sup> Figure 4 shows impulse *TDT* response at three temperatures (60 K, 40 K, 20 K), and at three biases (+2.5 V, +5 V, and -5 V) at 20 K. Qualitatively, the *TDT* response amplitude decreases (mainly due to an increase in impedance mismatch), and the delay increases (due to an increase in shunt capacitance) with decreasing temperature. To separate the intrinsic shunt losses from the impedance mismatch effect and the intrinsic dispersion from the low-pass filtering effect of the series coupling inductance, we used slightly modified forms of Eqs. (3) and (4) and impulse-*TDT* response data shown in Fig. 4 to calculate the attenuation  $\alpha$  and refractive index  $n$  as a function of frequency.

Once the YBCO electrodes are in the superconducting state (below about 86 K), the series resistive losses become negligibly small, and shunt losses (i.e.,  $G$ ) are expected to dominate dissipation in the waveguide. Between 85 K and 60 K, the total attenuation is immeasurably small and the waveguide is virtually dispersionless at least up to 2 GHz. Below 60 K, the waveguide exhibits dissipation that increases approximately linearly with frequency. The dissipation increases whereas the effective refractive index  $n$  decreases with bias.

Also, we note that  $n$  becomes dispersive (high frequency components propagate faster) at  $\pm 5$  V bias. Furthermore,  $n$  at 20 K seems to have a sharp drop at around 1 GHz - the exact frequency dependence is difficult to determine due to very small signal to noise ratio above 1 GHz.

The STO material is also known to be quite lossy at low temperatures. The attenuation due to the dissipation in the bulk of the dielectric is proportional to the dielectric loss tangent  $\tan\delta$ . We will make the assumption that the dielectric loss in STO dominates shunt losses in our waveguide structure in the whole range of the data shown in Fig. 4, except possibly above about 1 GHz at 20 K and 40 K.

No comprehensive model exists for dielectric losses in STO. Some possible mechanisms for microwave dielectric losses have recently been considered by Vendik, et al.<sup>16</sup> These loss mechanisms include the fundamental loss connected with multi-phonon scattering of the soft phonon mode, and the transformation of electromagnetic oscillations into acoustic oscillations due to residual ferroelectric polarization or charged defects. The fundamental loss mechanism predicts increasing loss with decreasing temperature below about 60 K and with increasing bias, similar to what we observe in our experiments. However, all three mechanisms also predict linear increase of loss tangent  $\tan\delta$  with frequency up to 100 GHz, in contrast to the frequency-independent behavior we have observed.

The Vendik model relies on the dielectric response of a system with a single degree of freedom.<sup>16</sup> However, this Debye<sup>17</sup> type description is inadequate to describe the response of a system with a distribution of relaxation times, i.e., with many degrees of freedom.<sup>18</sup> A general empirical modification of the Debye expression which accommodates a distribution of relaxation times leads to, under certain conditions, a frequency-independent loss tangent behavior in agreement with experiments on many strongly-interacting dielectric systems (i.e., systems with strong interactions among spin, charge, or lattice degrees-of-freedom).<sup>18</sup> Our observation here of a frequency-independent loss tangent implies that STO crystals need a more general treatment than that based on a weakly-interacting system.

### *LARGE-SIGNAL IMPULSE-TDT*

As we have shown in the previous sections, by applying a dc bias  $v_{dc}$ , we can change the small-signal electrical characteristics of our waveguides through changes in the shunt capacitance  $C$  and the shunt conductance  $G$ .

Since the lowest electrically-active transverse optic mode (or, soft phonon mode) in STO is expected to be of the order of a few hundred GHz, the dc bias effects should, ideally, provide all the information necessary for the determination of the large-signal behavior of the waveguide in the microwave frequency range up to the soft phonon mode frequency. In practice, however, such a relationship is complicated because our waveguide devices exhibit bias-dependent dispersive (i.e., bias- and frequency-dependent  $\epsilon_r$ ) and bias- and frequency-dependent dissipative effects at much lower frequencies -- in the frequency range of our interest between 0 and 2 GHz. Since the nonlinearity, the dispersion, and the frequency-dependent dissipation all cause pulse-shaping effects of some sort (in fact, it is the balance between dispersive and nonlinear effects that could give rise to stable pulse shapes, called solitons)<sup>19</sup>, it is necessary to distinguish among these effects for an accurate analysis of the large-signal behavior.

Figure 5 shows impulse TDT response for multiple transmissions with corresponding propagation distances of  $\ell$ ,  $3\ell$ , and  $5\ell$ , where  $\ell$  is the length of the waveguide. Since both the characteristic impedance mismatch between the waveguide and the external circuitry and the dissipation are quite large at 20 K, we expect the pulse within the waveguide to bounce back and forth between the device boundaries with only about 15% of the energy of the pulse being transmitted at either device boundary, but between about 50% to 90% of the overall energy being dissipated each time the pulse propagates a distance  $\ell$ . So, as a first approximation and ignoring frequency-dependent effects at the device boundaries, one may consider the transmitted pulses shown in Fig. 5 as sampling of the propagating pulse in an indefinitely long and uniform waveguide at different times. We see that, although the pulses get smaller and broader with time in all bias conditions, in the case of -2.5 V bias, the "triangular" shape of the pulse seems to be preserved. In other words, the pulse is shaped strongly by the waveguide when its amplitude is high, and this shape is somewhat preserved as the pulse makes a transition with time from large-signal to small-signal regime while the frequency-dependent dissipation acts on it.

We have previously developed a model in the form of a nonlinear wave equation describing the signal transmission in the large-signal regime.<sup>15</sup> This model was based on the small-signal measurements of delay time and pulse-broadening. Using these measurements to determine the nonlinearity and dispersion, we found that the validity of this model could be extended into the large-signal regime. The model was able to reproduce the basic pulse-shaping features experimentally observed. Its main flaw was that the dispersion effects seemed to be somewhat over-estimated.

Pursuing the philosophy that the small-signal results can be utilized to construct a model that also is valid in the large-signal regime, we will here use the improved measurements presented earlier to construct a correspondingly improved model of the nonlinear pulse-shaping.

There will be three components of this model; first there is the nonlinearity which is in the form of a bias-dependent shunt capacitance  $C$ . Secondly, the attenuation  $\alpha$  depends linearly on the frequency as  $\alpha = \alpha_0 \omega$  where  $\alpha_0$  is to be extracted from the measurements and will clearly depend on the bias voltage and the temperature. Finally, the frequency dependence of the refractive index is of the form  $n = n_0 - n_1 \omega$  which yields a contribution of the form  $\omega/k = u_0(v_{dc}) + u_1(v_{dc}) k$  to the dispersion relation. The next step is then to write down a model equation that reproduces these three characteristics in the linear (small-signal) limit. This is achieved by

$$\frac{\partial v_s}{\partial t} + u(v_{dc} + v_s) \frac{\partial v_s}{\partial x} = (\alpha \frac{\partial}{\partial x} + \beta \frac{\partial^2}{\partial x^2}) H\{v_s\} \quad , \quad (5)$$

where

$$H\{v_s\} = \frac{1}{\pi} \int_{-\infty}^{\infty} \frac{v_s(\xi)}{\xi - x} d\xi \quad (6)$$

is the Hilbert transform. In contrast to our earlier model,<sup>22</sup> we have here limited the model to describe propagation in one direction. This has been done for convenience and does not limit the generality of the model.

In the linear limit Eq. (21) has the dispersion relation

$$\omega = u(v_{dc})k - i\alpha|k| + \beta k|k| \quad (7)$$

which contains the components described above. The parameters  $\alpha$  and  $\beta$  are to be determined from the small signal results. The coefficients  $\alpha$  and  $\beta$  will depend parametrically on the bias voltage and the temperature.

As a test of the model we numerically simulate the pulse propagation for  $T = 20$  K for the cases  $v_{dc} = 0, -2.5$  V,  $+2.5$  V, and compare these results with those of the experiments shown in Fig. 5. In Fig. 6, we show examples of simulated pulses having propagated one, three and five device lengths  $\{$ . In the experiments, the pulse experiences frequency- and amplitude- dependent reflection and transmission at the boundaries, but we are neglecting this effect in the simulations. As seen, the model reproduces the overall features of the experimental data quite well even at rather large propagation distances. The simulations show that the “triangular” pulse shape for  $-2.5$  V bias is somewhat preserved as the pulse propagates, while the amplitude decreases and the width increases as a result of the dissipation. Since the dissipation plays a central role in Eq. (5), pure soliton solutions are not present, though, Eq. (5) in the absence of attenuation (i.e.,  $\alpha = 0$ ) probably supports soliton solutions due to its close relation to the Benjamin-Ono equation which is known to be exactly integrable. This is characteristic of soliton bearing equations.<sup>21</sup> Such soliton solutions of Eq. (5) would be interesting from a theoretical point of view since they will have algebraically decaying tails in contrast to more standard solitons with exponentially decaying tails – this will strongly influence their splitting and interactions properties.<sup>22</sup>

## CONCLUSION

As presented above, at low temperatures our HTS/NLD prototype devices exhibit strong dielectric nonlinearities and negligible series resistive losses from dc up to at least a few GHz, rendering them interesting for many applications at radio and microwave frequencies. Such potential applications fall into two broad categories: quasi-static and dynamic. Devices in the quasi-static category use the dielectric nonlinearity as a means of controlling the small-signal (linear) response of the device. A good example for this category is an electrically tunable multi-pole bandpass filter where dc or low-frequency control signals are used both to fine-tune the filter profile and to broadband-tune the passband for high-frequency signals.<sup>4</sup> In the dynamic category, devices are in the large-signal (nonlinear) regime, and thus can be used for harmonic generation and mixing,<sup>23</sup> parametric amplification,<sup>24</sup> pulse shaping,<sup>25</sup> etc. In this case, dc or low-frequency signals are used to control the nonlinear response. To have a realistic assessment of the potential of HTS/NLD materials in such broad ranges of applications, it is necessary to perform a broadband electrodynamic characterization in terms of not only nonlinear effects but also dispersive and dissipative effects.

The time-domain measurement and analysis technique we have developed in this study has allowed us to carry out such a comprehensive characterization. The 8-cm-long coplanar waveguides made from YBCO electrodes on single-crystal STO substrates have exhibited dielectric nonlinearity ( $\delta\epsilon_r/\epsilon_r V$ ) of about 1%/V at 60 K and more than 10%/V at 20 K. This nonlinearity was sustained at least up to 2 GHz at 60 K, and 1 GHz at 20 K, with corresponding frequency-independent effective  $\tan\delta$  values of less than  $10^{-3}$ , and about  $2 \times 10^{-2}$ , respectively. The waveguides, which were essentially dispersionless under zero bias, became dispersive under bias. With bias, the  $\tan\delta$  has also increased. At present, whether all these effects are caused by purely intrinsic properties of the STO material is unclear.

Finally, by using parameters determined from small-signal (linear) transmission characteristics of the waveguides as a function of dc bias, we have constructed a phenomenological nonlinear model equation. This equation -- combining nonlinearity with bias- and frequency-dependent dissipation, and bias-dependent dispersion -- has accurately predicted the large-signal (nonlinear) behavior such as pulse-shaping effects, which we have experimentally observed.

## Publications

1. Cai, D., et al., "A Perturbed Toda Lattice Model for Low Loss Nonlinear Transmission," *Physica D* **123**, 291 (1998).
2. Findikoglu, A.T., et al., "Electrodynamic Properties of Coplanar Waveguides Made from High-Temperature Superconducting  $\text{YBa}_2\text{Cu}_3\text{O}_{7-x}$  Electrodes on Nonlinear Dielectric  $\text{SrTiO}_3$  Substrates," *J. Appl. Phys.* **86**, 1558 (1999).
3. Findikoglu, A.T., et al., "Electrodynamic Properties of Single-Crystal and Thin-Film Strontium Titanate," (to be published in *Integ. Ferroelec.*).
4. Findikoglu, A.T., et al., "New Potential Applications of Nonlinear Dielectrics: Microwave Solitons and Stochastic Resonance," *Integ. Ferroelec.* **22**, 779 (1998).
5. Findikoglu, A.T., et al., "Pulse-Shaping Using Nonlinear Dielectric  $\text{SrTiO}_3$ ," *Appl. Phys. Lett.* **74**, 1770 (1999).
6. Jia, Q.X., et al., "Improvement in Performance of Electrically Tunable Devices Based on Nonlinear Dielectric  $\text{SrTiO}_3$  Using a Homoepitaxial  $\text{LaAlO}_3$  Interlayer," *Appl. Phys. Lett.* **73**, 897 (1998).
7. Jia, Q.X., et al., "Integrated Films for Josephson Junctions, SQUIDs and Electrically Tunable Microwave Devices," *Ceramic Trans.* **86**, 61 (1998).
8. Lu, P., et al., "Effects of Homo-Epitaxial  $\text{LaAlO}_3$  Layer on Microstructural Properties of  $\text{SrTiO}_3$  Films on  $\text{LaAlO}_3$  Substrates," *Thin Solid Films* **348**, 38 (1999).
9. Rasmussen, K.O., et al., "Higher-Order Effects on Shapiro Steps in Josephson Junctions," *Phys. Rev. B* **59**, 58 (1999).
10. Rasmussen, K.O., et al., "Soliton Motion in a Parametrically AC-Driven Damped Toda Lattice," *Phys. Rev. E* **58**, 6695 (1998).

## References

- [1] O. G. Vendik, L. T. Ter-Martirosyan, A. I. Dedyk, S. F. Karmanenko, and R. A. Chakalov, *Ferroelectr.* **144**, 33 (1993).
- [2] A. T. Findikoglu, Q. X. Jia, X. D. Wu, and D. W. Reagor, *Integr. Ferroelectr.* **15**, 163 (1997).
- [3] M. J. Lancaster, J. Powell, A. Porch, *Supercond. Sci. Tech.* **11**, 1323 (1998).

- [4] A. T. Findikoglu, Q. X. Jia, X. D. Wu, G. J. Chen, T. Venkatesan, and D. W. Reagor, Appl. Phys. Lett. **68**, 1651 (1996).
- [5] See pub. 4.
- [6] O. G. Vendik, Ferroelectr. **12**, 85 (1976).
- [7] S. Gevorgian, E. Carlsson, E. Wikborg, E. Kollberg, Integr. Ferroelectr. **22**, 765 (1998).
- [8] C. M. Jackson, J. H. Kobayashi, A. Lee, C. Prentice-Hall, J. F. Burch, and R. Hu, Micr. Opt. Tech. Lett. **5**, 722 (1992).
- [9] S. B. Herner, F. A. Selmi, V. V. Varadan, and V. K. Varadan, Mater. Lett. **12**, 424 (1993).
- [10] See pub. 6.
- [11] M. J. Dalberth, J. C. Price, C. T. Rogers, Mat. Res. Soc. Symp. Proc. **493**, 371 (1998).
- [12] See, for example, M. J. C. van Gemert, Philips Res. Repts. **28**, 530 (1973).
- [13] R. L. Kautz, J. Appl. Phys. **49**, 308 (1977).
- [14] See pub. 2.
- [15] See pub. 5.
- [16] O. G. Vendik, L. T. Ter-Martirosyan, and S. P. Zubko, J. Appl. Phys. **84**, 993 (1998).
- [17] P. Debye, *Polar Molecules* (Chemical catalog Co., New York, 1929).
- [18] R. M. Hill, and A. K. Jonscher, Contemp. Phys. **24**, 75 (1983).



- [19] See, for example, M. Remoissenet, *Waves Called Solitons* (Springer-Verlag, Berlin, 1994).
- [20] S. Havriliak, and S. Negami, J. Poly. Sci. **C14**, 99 (1966).
- [21] See pub. 1.
- [22] Y. Matsuno, Int. J. Mod. Phys. B **9**, 1985 (1995).
- [23] A. T. Findikoglu, Q. X. Jia, D. W. Reagor, and X. D. Wu, Electron. Lett. **31**, 1814 (1995).
- [24] P. K. Tien, J. Appl. Phys. **29**, 1347 (1958).
- [25] S. R. Wilson, M. M. Turner, and P. W. Smith, IEEE Trans. Electron. Devices **38**, 767 (1991).

## Figure Captions

FIG. 1. Schematic coplanar waveguide (CPW) device structure.

FIG. 2. Schematic measurement set-up.

FIG. 3. Electrical circuit model.

FIG. 4. Impulse *TDT* response at different temperatures (60 K, 40 K, 20 K), and biases (0 V, +2.5 V, +5 V, -5 V for 20 K).

FIG. 5. Large-signal impulse *TDT* response at 20 K for different biases (0 V, +2.5 V, -2.5 V) with zero, two, and four reflections (0-R, 2-R, 4-R) at device boundaries, with corresponding propagation lengths of  $\lambda$ ,  $3\lambda$ , and  $5\lambda$ , respectively.

FIG. 6. Simulated large-signal impulse *TDT* response at 20 K for different biases (0 V, +2.5 V, -2.5 V) with zero, two, and four reflections (0-R, 2-R, 4-R) at device boundaries, with corresponding propagation lengths of  $\lambda$ ,  $3\lambda$ , and  $5\lambda$ , respectively.

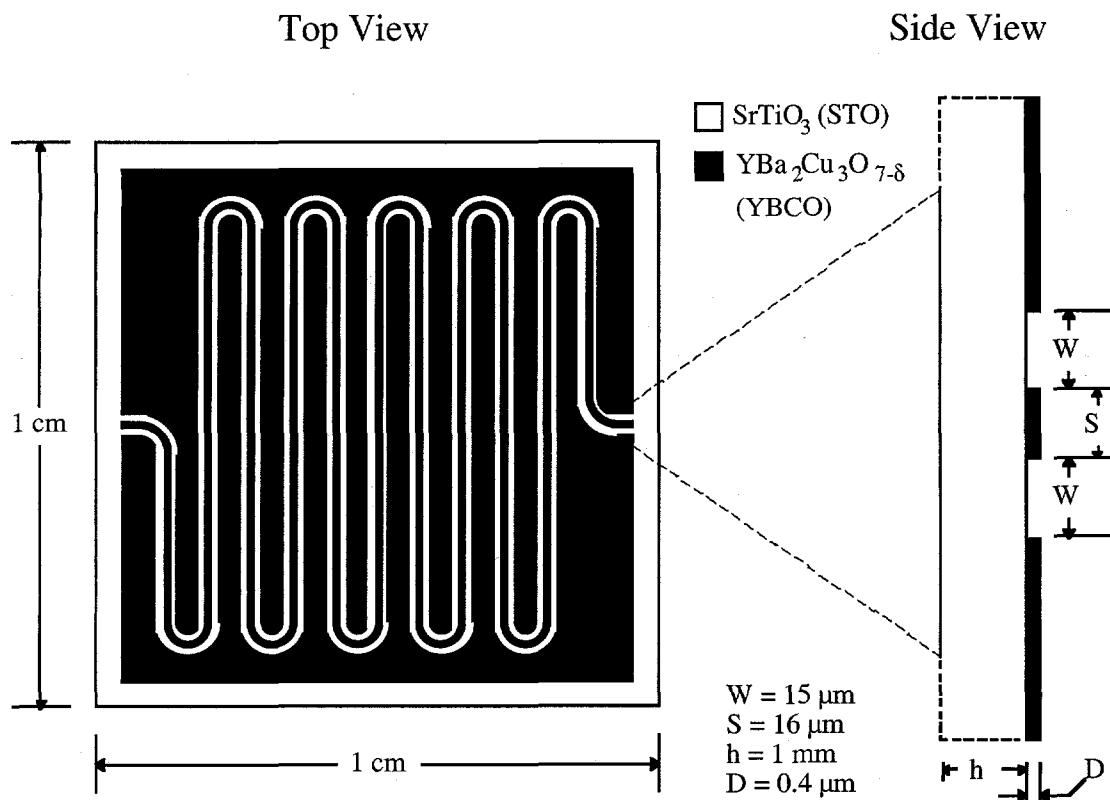


Fig. 1

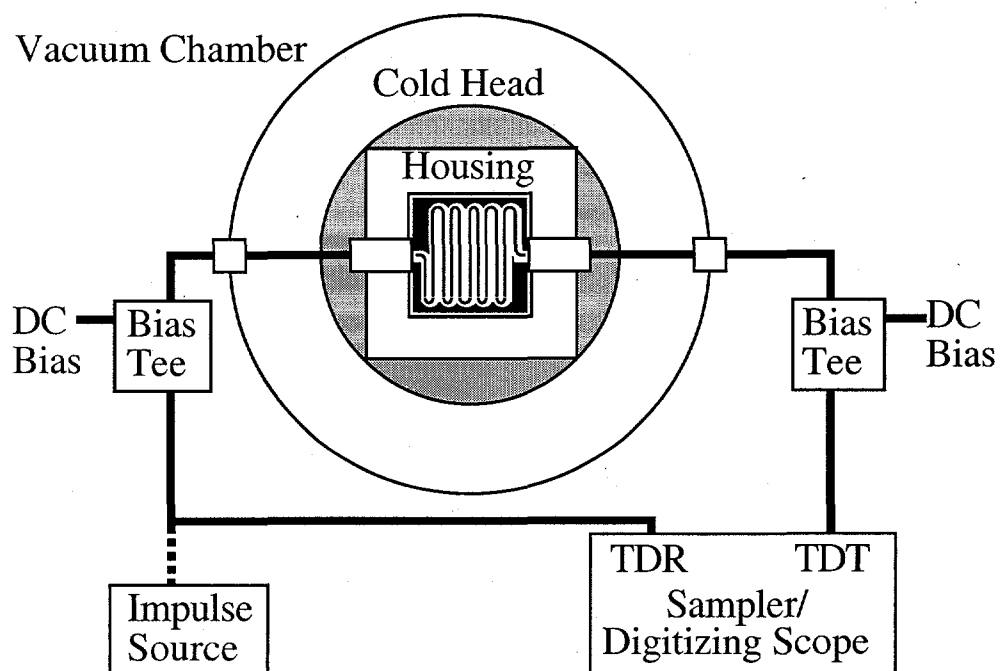


Fig. 2

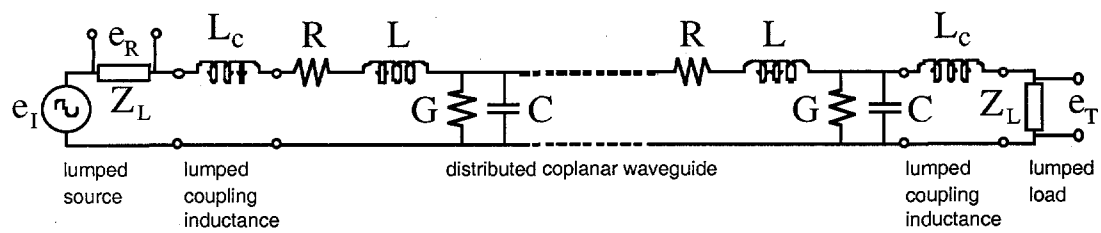


Fig. 3

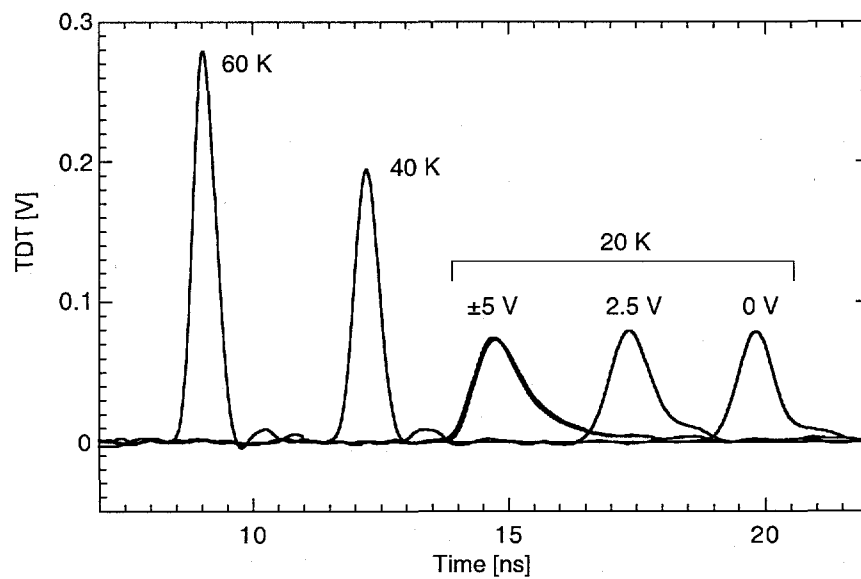


Fig. 4

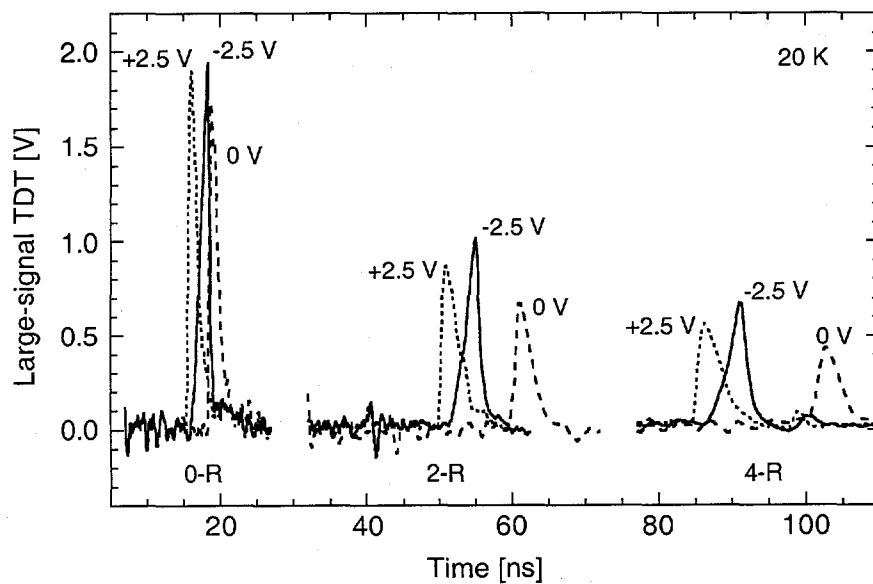


Fig. 5

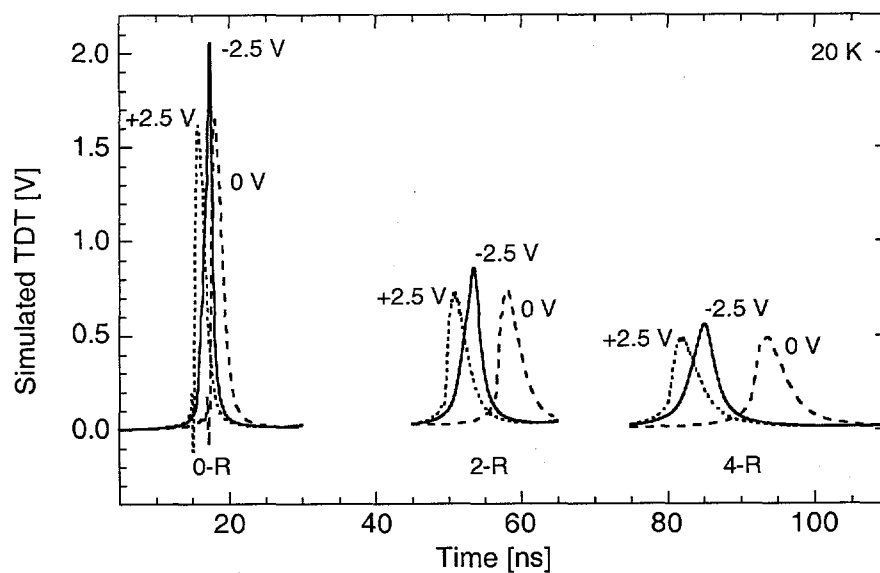


Fig. 6